Supporting Information to the Manuscript
"Single-Crystal Diamond Nanowire Tips for Ultrasensitive Force Microscopy"

Y. Tao[1,2] and C. L. Degen[1]

[1]Department of Physics, ETH Zurich, Otto Stern Weg 1, 8093 Zurich, Switzerland.

[2]Department of Chemistry, Massachusetts Institute of Technology, 77 Massachusetts Avenue, Cambridge MA 02139, USA.

1. Diamond Tip and Nanowire Fabrication

1.1. Diamond etching

Optical grade, ⟨100⟩-oriented single-crystal diamond plates (3 mm × 3 mm × 0.5 mm) were purchased from Element Six. ICP etcher used for this study was an Oxford Instruments ICP 180. We have used a 4-inch quartz carrier wafer through out this study. For the direct etching method, as-received samples were positioned at the center of the quartz carrier wafer and loaded into the ICP etcher. A 3 mm-tall macor frame with an inner 10 mm x 10 mm area was put around the diamond to prevent the latter from slipping off of the quartz carrier wafer during automatic robotic arm transfer between the loadlock and the main chamber. Samples were etched for 30 minutes in 10 mtorr O_2 (30 sccm) using 2100 W ICP and 100 W bias powers. It has been our experience that ICP etching rates typically vary by a factor up to 2-3 when executing an identical recipe on different instruments, even with etchers of the same model. Therefore, the conditions reported here should only serve as a starting point guideline for instrument-specific fine tuning. We have also noticed significant interference between recipes from different users. It is recommended that chamber cleaning and preconditioning runs of at least 30 minutes be performed before etching experiments on diamond samples.

To fabricate pillars with lithographic placement, we first cleaned the samples in a boiling piranha solution for 10 minutes. They were then glued to a silicon carrier chip using a thin layer of G1 Epoxy (Gatan). Care was taken to use as little glue as possible while still obtaining a continuous film between the diamond and the silicon. This care was to increase the resistance of the glue to both wet and dry etching steps by decreasing the width for convective access. The glue was cured at 100°C over 1 hour. After the gluing, the samples were etched in buffered HF for 2 minutes in order to remove adventitious micromasks, rinsed in DI water, dipped into boiling piranha solution for 10 seconds, and finally blown dry with nitrogen gas after DI water rinsing. The samples were coated with a double layer of PMMA-PMAA/PMMA resist stack to facilitate lift off. The thickness of the

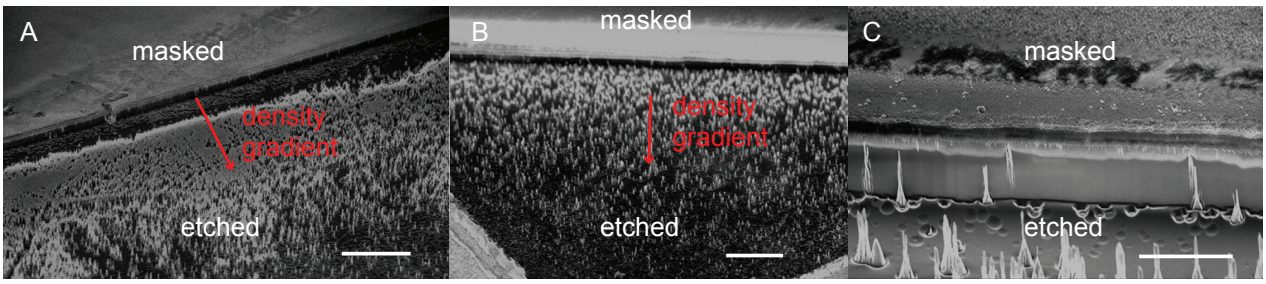

Figure S1: Testing the Micromasking Mechanism for Spontaneous Pillar Formation (A)-(B) SEM micrographs of samples etched by covering part of the diamond surface with a glass cover slip. (C) Zoom-in at where the edge of the glass cover slip mask had been. Scale bars are 50 μm in (A)-(B) and 10 μm in (C).

bottom PMMA-PMAA layer was 800 nm, and the thickness of the upper PMMA layer was 150 nm. 8 nm of Au was evaporated on top of the resist by ebeam evaporation to serve as the charge-dissipation layer during ebeam lithographic exposure. After exposure and resist development, 500 nm of Al_2O_3 was deposited by ebeam evaporation at a rate of 0.5 nm/sec. Liftoff was performed by leaving the samples in acetone without agitation. ICP etching was performed with 2500 W ICP and 40 W bias powers for 30 minutes. To pinch off the waist of the resulting pillars, the sample was subjected to 10 more minutes of etching using 2500 W ICP and 60 W bias powers.

1.2. Micromasking

To test whether the appearance of diamond pillars during ICP etching could have been caused by the presence of masking impurities, we performed an experiment by masking part of a diamond sample using microscope glass cover slip that was 180 μm in thickness. A density gradient of pillars is clearly visible, as indicated in Figure S1A-B. As a result, the micromask could be silicon dioxide from the quartz carrier wafer, which is a good hardmask material for diamond etching in oxygen plasma. We also notice that at the immediate vicinity of where the glass mask had been, there is a depletion of pillar density. This is despite the fact that diamond etching at this location had taken place at the same rate as at other exposed locations. We attribute the result to the existence of a certain trajectory of micromask falling from on top of the glass cover slip. The macroscopic analogue would be for people to run for cover toward the edge of a cliff during an earthquake, so that falling boulders had smaller chances of hitting them.

1.3. Mechanism of nanowire and tip formation

The shape of the spontaneously formed pillars was likely controlled by different etching anisotropy mechanisms. ICP etching is inherently an anisotropic technique that favors the formation of structures with sidewalls parallel to substrate normal. A close inspection of the shape of the pillar bases suggested the additional presence of chemical etching anisotropy; many pillar bases distinctly showed

what appeared to be crystallographic planes. The bases roughly exhibited four-fold symmetry with surface normal that seemed to point in the $\langle nn1 \rangle$ direction, where $n > 1$. The experimentally obtained high-index planes were likely the result of a kinetic balance between chemical etching anisotropy and physical sputtering. For example, pure chemical etching might favor the formation of {111} planes due to the better bonding of surface carbons to the underlying lattice, as previously reported in H_2 etching of diamond [1]. The physical sputtering effect during ICP etching would tend to tilt the surface normal of {111} planes toward the $\langle 110 \rangle$ directions. Additional shaping effects may include local concentration variation of reactive radical and ionic species. Diffusion and geometry-dependent charging would create such local concentration inhomogeneity, which may explain the rounding off of edges. Together, these effects are qualitatively consistent with the experimentally observed result.

A second cause based on electron shading effects would also explain the formation of conical bases [2]. It could in addition account for the thinning of the waist half way up a nanopillar. In plasma etching, electrons and positive ions bombarding the etched surface do not have the same angular velocity distribution. Positive ions such as O_2^+ have a velocity distribution biased heavily perpendicular to the surface. Electrons, on the other hand, have an almost uniform angular distribution. This wide distribution of impact directions causes the tips of pillars to efficiently block and trap a larger total flux of negative charge raining down at it from 360°. When the pillar is insulating, which is the case for diamond, significant negative charge build up near the tips of the pillars in the steady state. This accumulation of negative charge in turn leads to a bending of the trajectories of positive ions passing nearby inward toward the pillar shaft. This bending of positive ion trajectory increases bombardment of the middle portion of the pillar by reactive species, causing it to be etched faster. A concurrent consequence of this increased influx of positive ions is a gradual change from net negative to a net positive charge accumulation moving down from the tip toward the base. At a certain point, the lower regions of the pillar would have become so positively charged that it would start to repel the positive ions. This second ion trajectory bending event would explain the fanning out of the base into a cone and the formation of a circular trench around it.

1.4. Attachment of diamond nanowires to silicon cantilevers

To facilitate visualization and micromanipulation under an optical microscope, we first transferred the diamond nanowires from the starting diamond substrate to a silicon wafer chip. A small piece of sticky Gel-Pak 4 material was broken off from the box using tweezers. The piece of gel was put on top of the donor diamond surface, and pressed tight with tweezers. The gel was peeled away and stamped on a clean silicon wafer chip at several locations. An example of optical image

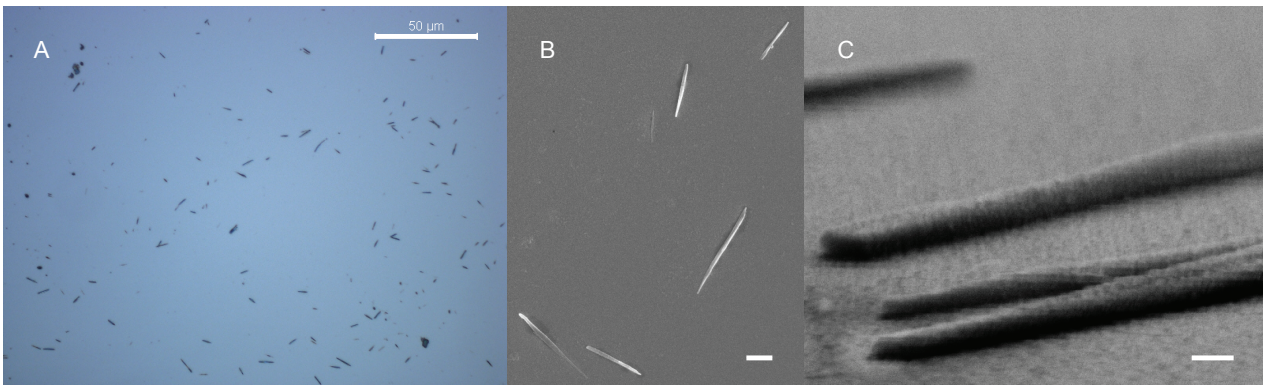

Figure S2: Transfer of Diamond Nanowires to a Silicon Substrate (A) Optical micrograph of long diamond nanowires freshly transfered to a silicon substrate. (B)-(C) SEM micrographs of diamond nanowire on silicon. In this example, diamond nanowires had been further coated with 15 nm YF_3 and 10 nm Pt for other reasons. Scale bars are 50 μm in (A), 1 μm in (B), and 100 nm in (C).

of freshly-transferred sample is shown in Figure S2. The nanowires in this batch seemed to have roughly rectangular cross-section. We note that while we have not pursued the idea further, it should be possible to tune etching conditions to enable longer etches to obtain nanowires that are suitable to be used as mechanical resonators themselves. Wire length 10 μm is certainly possible. The oblong cross-sectional shape of the nanowires makes them ideal nanowire mechanical oscillators with well-separated and stable mechanical modes [3].

To mount nanowires onto silicon cantilevers, we used a commercial micromanipulator system (Narishige Three-axis Hanging Joystick Oil Hydraulic Micromanipulator, model: MMO-202ND). A glass capillary (Narishige Model: G1) was pulled to two tips under a heating power of 56.5 using a capillary puller (Narishige, Model: PC-10). Resulting capillary tip radius was around 500 nm. The tip was used to nudge a NW on the silicon substrate and to move it into an orientation that was either perpendicular or parallel to the capillary tip axis. For longer wires ($> 5\,\mu$m), parallel orientation was preferable. For shorter wires, only the perpendicular orientation worked well for the subsequent re-deposition step. The capillary was pressed into the diamond nanowire, often repeatedly, until the latter stuck to the capillary and got lifted off of the surface. The capillary tip was retracted from the surface and cantilever chip was brought close to the microscope focal point. Note that we had previously deposited a dab ($\approx (1\mu\text{m})^3$) of G1 epoxy (5:1 glue:hardener) at the tip of the cantilever. Cantilever chip was oriented so the cantilever was parallel to the xy plane projection of the diamond nanowire on the capillary tip. The nanowire was brought into contact with the silicon tip, the sticking force with the glue was generally stronger than the van der Waals force with the capillary tip, allowing the nanowire to stay on the cantilever as the micromanipulator tip was gently moved away in a direction parallel to the Si cantilever. The glue was allowed to cure at room temperature over 24h.

1.5. Silicon Cantilever Pretreatment

To increase the intrinsic mechanical quality factor of the silicon cantilever, we subjected it to a surface chemical treatment as reported elsewhere [4,5]. For this particular experiment, we had chosen to use propyne as the reagent gas. The procedure generally results in a reduction of intrinsic friction at 4K by a factor of 2-5, depending on the recipe used and the air exposure time between preparation and the start of vacuum pumping.

2. Measurements of Noncontact Friction

The mechanical properties of a DNW-tipped Si cantilever and its interaction with a gold surface were measured in a custom-built scanning force microscope designed for magnetic resonance force microscopy [6]. After surface treatment for intrinsic friction reduction, cantilevers were equipped with DNW under ambient conditions and then mounted in a high-vacuum chamber ($< 10^{-6}$ mbar) at the bottom of a dilution refrigerator ($\sim 65\,\mathrm{mK} - 300\,\mathrm{K}$). The distance between the cantilever tip and a gold surface mounted on a 3D piezo walker-scanner (Attocube) was decreased to within 10 μm by monitoring through a stereo microscope. The high-vacuum chamber was closed and evacuated to $< 10^{-6}$ mbar.

When vacuum was sufficiently deep to allow for coherence vibration of the cantilever, its motion was detected using a low-power fiber-optic interferometer [7] operating at a wavelength of 1550 nm and producing less than 10 nW of laser light incident at the cantilever. Cantilever was actuated by a piezo actuator and its motion was controlled by a custom self-oscillation control loop implemented in Labview FPGA (National Instruments). We oscillated the cantilever at a constant oscillation amplitude of 5 nm while further decreasing the distance between the tip and the surface. Physical contact between the two led to the disappearance of the mechanical peak (7 kHz) from the spectrum. Concurrently, there was the appearance of another peak (≈20 kHz) in the spectrum, likely due to the cantilever oscillating as a doubly-clamped device when the tip is fixed by the tip-surface contact point. In order to determine the reliability of the x axis in Figure 4 of the main text, we performed repeated touch down at the same (x, y) location in 2-Å steps. We find that the there is a spread in the actually obtained value. Standard deviation was measured to be 0.54 nm. This value is small enough for us to be confident of the main conclusions of the study that no measurable noncontact friction was observed above 10 nm.

Resonator frequency f_c and quality factor Q were measured using the ring-down method [8], and the spring constant k_c calibrated via a thermomechanical noise measurement at room temperature [9]. To exclude cavity effects, it was verified that the same Q factor was obtained whether the measurement

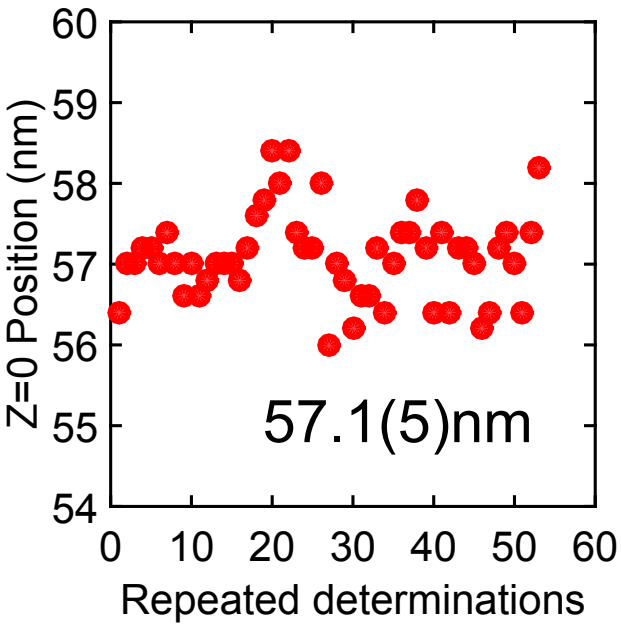

Figure S3: Determination of the Reliability of the $z = 0$ Point. The cantilever was repeatedly approach to the surface until physical contact. The y axis is z piezo extension needed to induce the touching. The results shows that the standard deviation was below 1 nm.

was done on the positive or negative (red- or blue-shifted) side of the interferometer fringe.

References

[1] Cheng, C.-L., Chang, H.-C., Lin, J.-C., Song, K.-J., and Wang, J.-K. *Phys. Rev. Lett.* **78**, 3713–3716 (1997).

[2] Giapis, K. In *Handbook of Advanced Plasma Processing Techniques,* Shul, R. and Pearton, S., editors. Springer (2000).

[3] Nichol, J. M., Naibert, T. R., Hemesath, E. R., Lauhon, L. J., and Budakian, R. *Phys. Rev. X* **3**, 031016 (2013).

[4] Tao, Y., Navaretti, P., Hauert, R., Grob, U., Poggio, M., and Degen, C. L. *Nanotechnology* **26**, 465501 (2015).

[5] Tao, Y., Hauert, R., and Degen, C. L. *submitted* (2015).

[6] Rugar, D., Budakian, R., Mamin, J. H., and Chui, B. W. *Nature* **430**, 329 (2004).

[7] Rugar, D., Mamin, H. J., and Guethner, P. *Appl. Phys. Lett.* **55**, 2588–2590 (1989).

[8] Yasumura, K. Y., Stowe, T. D., Chow, E. M., Pfafman, T., Kenny, T. W., Stipe, B. C., and Rugar, D. *J. Microelectromech. Sys.* **9**, 117 (2000).

[9] Stowe, T. D., Yasumura, K., Kenny, T. W., Botkin, D., Wago, K., and Rugar, D. *Appl. Phys. Lett.* **71**, 288 (1997).